Microchimica Acta (2019) 186: 829
https://doi.org/10.1007/s00604-019-3962-z

ORIGINAL PAPER

Titanium(IV)-functionalized zirconium-organic frameworks as dual-metal affinity probe for recognition of endogenous phosphopeptides prior to mass spectrometric quantification

Haoyang Zheng[1] · Jiaxi Wang[1] · Mingxia Gao[1] · Xiangmin Zhang[1]

Received: 11 June 2019 / Accepted: 18 October 2019 / Published online: 21 November 2019

Abstract

A zirconium-organic framework was modified with titanium(IV) ions to obtain a modified framework that is shown to be a viable sorbent for selective capture of phosphopeptides. This dual-metal affinity probe exhibits 0.1 fM limits of detection and excellent size-exclusion effect (the mass ratio of β-casein digests/BSA/intact β-casein is 1:1000:1000). This is attributed to abundant Ti(IV) and Zr(IV) coordination sites and high porosity. The performance of the sorbent for extracting endogenous phosphopeptides from human serum and saliva was investigated. Especially, 105 endogenous phosphopeptides from saliva were captured specifically. In addition, the amino acid frequency of the enriched phosphopeptides was analyzed. Conservation of sequence around the identified phosphorylated sites from saliva confirmed that phosphorylation took place in the proline-directed motifs.

Keywords Metal-organic frameworks · Nanomaterials · Post-functionalization · Dual-metal ions · Size-exclusion · Human saliva · Phosphoproteome · MALDI-TOF MS · Immobilized metal ion affinity chromatography · Post-translational modification

Introduction

Reversible phosphorylation is a key mechanism regulating signal transduction in biological processes. Many diseases are associated with abnormal phosphorylation of protein at specific sites [1, 2]. Global and exhaustive analysis of protein phosphorylation sites is crucial that can assist us in looking for potential biomarkers related to cancers. Mass spectrometry (MS)-based phosphoproteomics analysis becomes the most attractive strategy due to its high throughput [3]. Substoichiometric abundance and low ionization efficiency of phosphopeptides, however, impedes direct detection through MS [4–8]. As a result, enrichment and separation of phosphopeptides prior to MS analysis is prerequisite.

Various strategies have been developed to specifically capture phosphopeptides from complex biosamples, including solid-phase extraction (SPE) [9], strong cation exchange chromatography (SCX) [10], metal oxide affinity chromatography (MOAC) [11] and immobilized metal affinity chromatography (IMAC) [12, 13]. Due to the high affinity between metal and phosphoate groups, MOAC and IMAC methods have been utilized for enriching phosphopeptides extensively. Each metal extracts a unique set of phosphorylated peptides, causing distinct phosphorylation profile for same organism [14]. To increase coverage of phosphorylated peptides, materials functionalized with various metal ions that exhibit complementary capture ability, have been exploited as phosphopeptides affinity probe (PPAP) [15]. In addition, high porosity that endows PPAPs with the function of size-exclusion is also vital [16–18], especially for enriching endogenous phosphopeptides from complex biosamples. High abundance and large molecular weight proteins can always be found in them. It is necessary to fabricate novel porous materials with multi-metal ions

Electronic supplementary material The online version of this article (https://doi.org/10.1007/s00604-019-3962-z) contains supplementary material, which is available to authorized users.

✉ Mingxia Gao
mxgao@fudan.edu.cn

[1] Department of Chemistry and Institutes of Biomedical Sciences, Fudan University, Shanghai 200433, China

for extracting endogenous phosphopeptides from organism.

Metal-organic frameworks (MOFs) have been developed rapidly in many fields, including gas separation [19], catalytic degradation [20], luminescence sensing [21, 22] and drug delivery [23]. Remarkably broad applications should be attributed to their high surface areas, tunable properties and further modification. MOFs have also been applied in phosphopeptides enrichment because of the existence of metal centers and high porosity [24]. However, single metal ion and limited coordination sites cause that extraction of phosphorylated peptides, through MOFs without further modification, has low selectivity [17]. Immobilizing other metal ions on parent MOFs, which creates more abundant metal sites, provides a solution for such a predicament. For example, Peng et al. fabricated a novel dual-metal centered MOF for specifically enriching phosphopeptides via covalent-coordination cooperative modification of Uio-66-NH_2 [18]. Liu et al. synthesized core-shell multi-sites MOF as phosphopeptides affinity probe by titanium atom exchange with zirconium atom inside Uio-66 [16]. Despite of the effort to prepare multi metal-based MOFs for PPAP, the above mentioned synthesized approaches need multi-steps or harsh reaction condition, which can lead to the collapse of frameworks. In a consequence, developing a novel modification strategy is extremely urgent for fabricating multi-metal MOF as PPAP.

Titanium(IV) is one of the most promising candidates for extracting phosphopeptides from intricate biosamples, because of its robust affinity with phosphoate. Consequently, titanium ions functionalized zirconium-organic framework (Ti^{4+}@Zr-MOF) was prepared at mild reaction condition through Ti^{4+} chelation to bipyridine chelation sites within Zr-MOF. This dual-metal PPAP that possessed more abundant coordination sites showed better phosphopeptides extraction efficiency compared with parent Zr-MOF. Due to the vast interaction with phosphopeptides and open 3D frameworks of Ti^{4+}@Zr-MOF, it exhibited ultra-low limit of detection and outstanding size-exclusion effect towards capture of phosphopeptides. As expected, for practical application, when human serum and saliva were incubated with Ti^{4+}@Zr-MOF, 4 endogenous phosphopeptides and 105 endogenous phosphopeptides were identified respectively. Amino acid frequency of the captured phosphopeptides by Ti^{4+}@Zr-MOF from saliva was analyzed. The results uncovered that phosphorylation occurred at proline-directed motifs, which provided the awareness of kinase recognition in salivary proteins. Ti^{4+}@Zr-MOF with robust affinity to phosphopeptides has great potential for large-scale phosphoproteomics research.

Experimental section

Materials and reagents

Zirconium tetrachloride ($ZrCl_4$), terephthalic acid (TPA), tetraisopropoxytitanium (TIPT) and 2,2′-bipyridine-5,5′-dicarboxylic acid (H_2bpydc) were purchased from Adamas-beta (http://www.adamas-beta.com). Trifluoroacetic acid (TFA), 2,5-dihydroxybenzoic acid (DHB), α-Casein, β-Casein, bovine serum albumin (BSA) and trypsin from bovine pancreas were purchased from Sigma-Aldrich (https://www.sigmaaldrich.com, USA). Acetonitrile (ACN) was purchased from Merck (https://www.merckgroup.com, Darmstadt, Germany). Milli-Q water (http://www.merckmillipore.com, Millipore, Bedford, MA) was used in all process. All of the other starting materials and reagents were also purchased from commercial sources and used without further purification. Human serum and saliva were obtained from Shanghai Zhongshan Hospital.

Instrumentation

The power X-ray diffraction (PXRD) were recorded with a Bruker D8 Advance diffractometer using Cu$K\alpha$ radiation with 40 mA and 40 kV, with a scan range of 2 theta from 5° to 50°. Fourier transform infrared spectra (FTIR) were collected on a Nicolet IS10 infrared spectrum radiometer in the range of 4000–400 cm^{-1} using the KBr pellets. X-ray photoelectron spectra (XPS) were obtained on a Perkin Elmer PHI 5000C & PHI 5300 system by using the Mg$K\alpha$ anode. All binding energies were calibrated by using contaminant carbon(C 1 s = 284.6 eV). Nitrogen adsorption/desorption isotherms were measured at liquid nitrogen temperature using a Tristar 3020 analyser. Thermogravimetric analysis (TGA) was measured using a TGA 8000 system at a heating rate of 5 K min^{-1} under nitrogen protection. Energy dispersive X-ray (EDX) was performed on Philips XL30. Transmission electron microscopy (TEM) images were taken on JEOL 2011 microscope.

Preparation of Zr-MOF and Ti^{4+}@Zr-MOF

Zr-MOF was synthesized according to previous reported method [25] with some modifications. Detailed procedures to synthesize Zr-MOF are displayed in Electronic Supporting Material. Ti^{4+}@Zr-MOF composite was prepared by soaking Zr-MOF (100 mg) into 20 mL methanol solution of $Ti(SO_4)_2$ (0.1 mM) for 6 h at room temperature under stirring. The resultant Ti^{4+}@Zr-MOF was washed with methanol fully. The product was then dried at 50 °C for 12 h under vacuum.

Preparation of Al^{3+}@Zr-MOF and Fe^{3+}@Zr-MOF

To compare the enrichment efficiency of Ti^{4+} with other metal ions, Al^{3+} and Fe^{3+} were also introduced into the parent MOFs (denoted as Al^{3+}@Zr-MOF and Fe^{3+}@Zr-MOF, respectively). Al^{3+}@Zr-MOF and Fe^{3+}@Zr-MOF was fabricated similarly to Ti^{4+}@Zr-MOF besides that $Ti(SO_4)_2$ was displaced by the same mole of $AlCl_3 \cdot 6H_2O$ and $FeCl_3 \cdot 6H_2O$ correspondingly.

Preparation of MIL-53(Al), MIL-53(Fe) and MIL-125(Ti)

To compare the enrichment efficiency towards phosphopeptides with single metal-based MOF, typical series MOF of Materials Institut Lavoisiers (MIL-53(Al), MIL-53(Fe) and MIL-125(Ti)) that have uniform organic linker terephthalic acid (TPA), were also prepared. MIL-53(Al), MIL-53(Fe) and MIL-125(Ti) were fabricated via solvothermal approach by mixing TPA and corresponding metal salts. For MIL-53(Al), 0.151 g $AlCl_3 \cdot 6H_2O$ and 0.104 g TPA were mixed in 7.5 mL DMF. After being stirred vigorously, the mixture was transferred into 20 mL Teflon-lined stainless steel container and heated at 180 °C for 12 h. The resulting powder was washed with DMF for three times and dried in vacuum. For MIL-53(Fe), the synthesized process was same as MIL-53(Al) except that the metal ions were replaced by Fe^{3+}. MIL-125(Ti) was prepared via reported protocol [26] with some modifications. The concrete process to fabricate MIL-125(Ti) was also depicted in Electronic Supporting Material.

Digestion of standard proteins and preparation of human serum and saliva

The standard β-casein, α-casein phosphoprotein and BSA were dispersed into 25 mM NH_4CO_3 buffer and heated at 100 °C for 10 min. After cooling down to 25 °C, trypsin was added into the solution at an enzyme/substrate ratio of 1:40 (*w*/w). The mixture was then incubated at 37 °C for 16 h under shaking. The digests were diluted to certain concentration for further enrichment process.

Human serum and saliva sample were prepared in similar methods. 1 mL serum or saliva were diluted with 1 mL 0.2% TFA and centrifuged for 10 min at the speed of 5000 rpm. The supernatant were collected for further utilization.

Selective enrichment of phosphopeptides from standard peptides with Ti^{4+}@Zr-MOF

200 μg Ti^{4+}@Zr-MOF were dispersed into 100 μL loading buffer (ACN/H_2O/TFA = 50/48/2) containing standard phosphoprotein digests. The suspension was incubated at 37 °C for 30 min. After being separated by centrifugation, the materials were washed with 100 μL loading buffer for three times. Subsequently, the captured phosphopeptides were eluted by 10% $NH_3 \cdot H_2O$ for 20 min. Finally, the eluent was mixed with matrix solution for MALDI-TOF analysis.

For complex biosamples, 200 μg Ti^{4+}@Zr-MOF was suspended in loading buffer which contains 10 μL human serum or saliva. Then, the enrichment, washing and eluting process was the same as standard digests. The final eluent was analyzed by MALDI-TOF directly or lyophilized for next nano-LC-MS/MS analysis.

MS analysis and data search

Detailed procedures of MALDI-TOF and nano-LC-MS/MS analysis are shown in support information. Data search are also listed in support information.

Results and discussion

Choice of materials

Among the thousands of reported MOFs, Zr-based MOFs with excellent thermal and chemical stability are suitable for post-functionalization. More important, they can be explored as sorbents for extracting phosphopeptides. On the other hand, H_2bpydc as organic linkers can anchor other metal ions that is attributed to its 2,2′-bipyridyl moiety [27]. Therefore, the reaction of $ZrCl_4$ with H_2bpydc was carried out via solvothermal method to prepare parent Zr-MOF. To take advantages of free Lewis basic sites, titanium (IV) ions, possessing robust affinity with phosphoate and complementary extraction ability with Zr^{4+} [14], were encapsulated into Zr-MOF (Ti^{4+}@Zr-MOF) through chelation interaction. To confirm better capture efficiency of titanium (IV) ions towards phosphopeptides compared with other IMAC ions, Fe^{3+}@Zr-MOF and Al^{3+}@Zr-MOF were also synthesized and utilized for enriching phosphopeptides. In addition, three analogous single-metal MOFs (MIL-53(Al), MIL-53(Fe) and MIL-125(Ti)) were prepared as PPAPs too, which have uniform organic linker terephthalic acid (TPA) [26]. Their enrichment efficiency were compared with the corresponding dual-metal MOF in order to pinpoint the dual-metal synergistic effects.

Synthesis and characterization Ti^{4+}@Zr-MOF

The procedure for synthesis of post-functionalized Ti^{4+}@Zr-MOF is presented in Scheme 1a. In brief, zirconium-based MOF (Zr-MOF) possessing abundant chelation sites and robust rigidity was selected as the parent MOF. Subsequently, Ti^{4+} was introduced into Zr-MOF through coordination post-synthesized modification. Zr-MOF was fabricated via solvothermal strategy by mixing H_2bpydc and $ZrCl_4$ at 120 °C according to previous

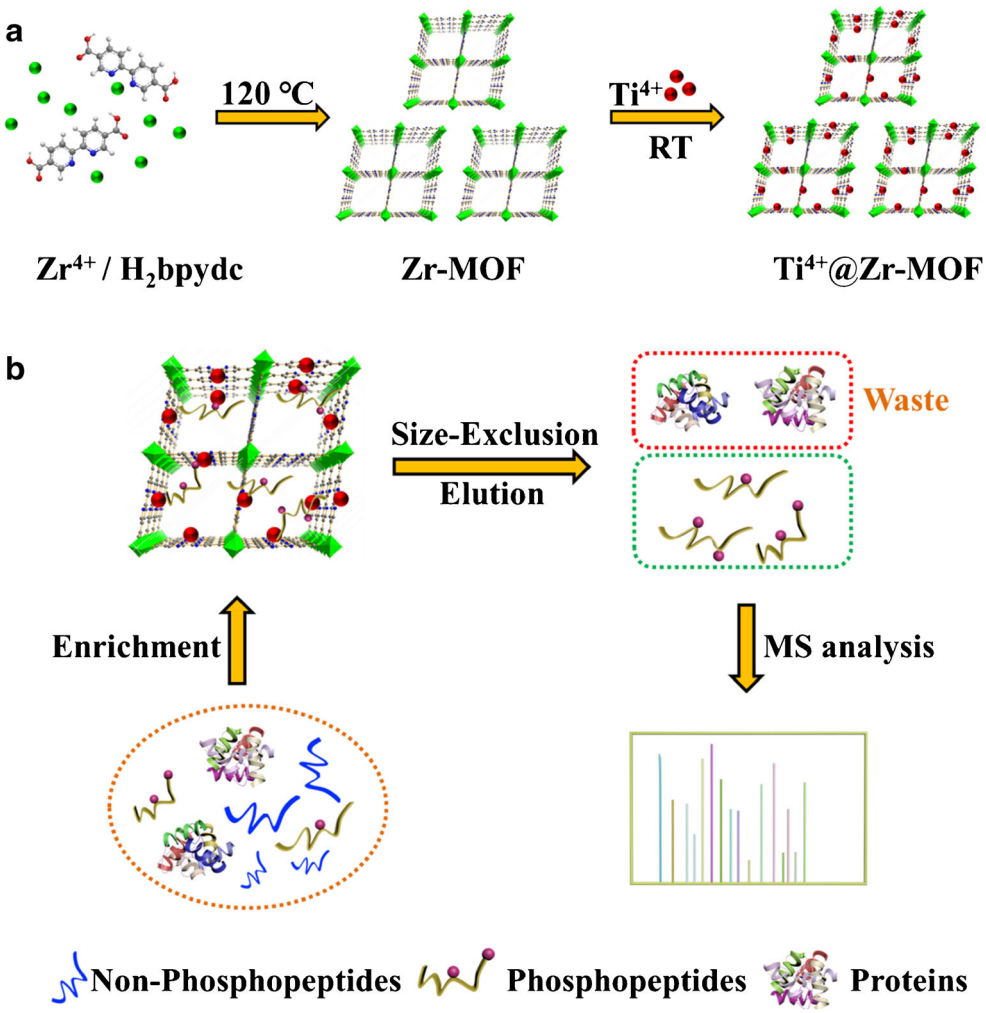

Scheme 1 **a** Schematic presentation of the synthesized approach of Ti^{4+}@Zr-MOF. (H_2bpydc is the acronym of 2,2′-bipyridine-5,5′-dicarboxylic acid; green balls represents Zr^{4+} and red balls represents Ti^{4+}) (**b**) Schematic presentation of the enrichment route of phosphopeptides (MS analysis is the acronym of mass spectrometric analysis)

reports [25]. Power X-ray diffraction (PXRD) pattern (Fig. 1a) agrees well with the simulated one, which confirms the successful synthesis of Zr-MOF. Ti^{4+}@Zr-MOF was prepared via incorporating Ti^{4+} into bipyridine sites of Zr-MOF through post-synthesized modification (PSM). The PXRD pattern (Fig. 1a) of Ti^{4+}@Zr-MOF is similar to the parent Zr-MOF, which suggests that the encapsulation of Ti^{4+} has little influence to the 3D frameworks. EDX (Fig. S1) was performed to certificate the successful introduction of Ti^{4+}. The atomic percentage and weight percentage of Ti^{4+} are 1.60 and 4.32 (Table S1), respectively. N_2 adsorption-desorption isotherms of Ti^{4+}@Zr-MOF are shown in Fig. S2a. It shows porosity towards N_2 and the Brunauer-Emmett-Teller (BET) surface area derived from isotherms is calculated as 158 m^2 g^{-1}. The pore size of Ti^{4+}@Zr-MOF is 1.3 nm (Fig. S2b) that is consistent with the parent Zr-MOF which holds the tetrahedral cages and the octahedral cages with the diameter of 1.2 nm and 1.6 nm [25], respectively. The analogous pore size also indicates intact rigidity after Ti^{4+} was encapsulated into Zr-MOF.

In order to confirm Ti^{4+} is coordinated with bipyridine sites rather than physical absorption within the pore, FTIR and XPS were performed. As shown in Fig. 1b, comparing with the IR spectra of Zr-MOF and Ti^{4+}@Zr-MOF, the stretching vibration of C=N is shifted from 1658 cm^{-1} to 1689 cm^{-1}. This should be attributed to the coordination interaction between Ti^{4+} and bipyridine sites, which hinders the vibration of C=N. Then, XPS analysis was also carried out to prove the interactions between loaded Ti^{4+} and bipyridyl moieties. The spectra of Ti^{4+}@Zr-MOF (Fig. 1c) appear the peak of Ti $2p^3$ that can't be detected in the Zr-MOF, suggesting the successful encapsulation of Ti^{4+}. The binding energy of Ti $2p^3$ of Ti^{4+}@Zr-MOF is lower than the $Ti(SO_4)_2$ (Fig. 1d), implying the different coordination environment of Ti^{4+}. On the other hand, the binding energy of N 1 s in the spectra (Fig. S3) of Ti^{4+}@Zr-MOF also has a slight shift compared to primitive Zr-MOF. The above results reflect that Ti^{4+} is supposed to coordinate with bipyridine sites within Zr-MOF instead of adsorption. Transmission electron microscopy demonstrates the octahedral-shaped crystals of Zr-MOF and it has nanoscale dimensions (Fig. 1e). No obvious change of morphology was observed when Ti^{4+} is coordinated with bipyridine sites

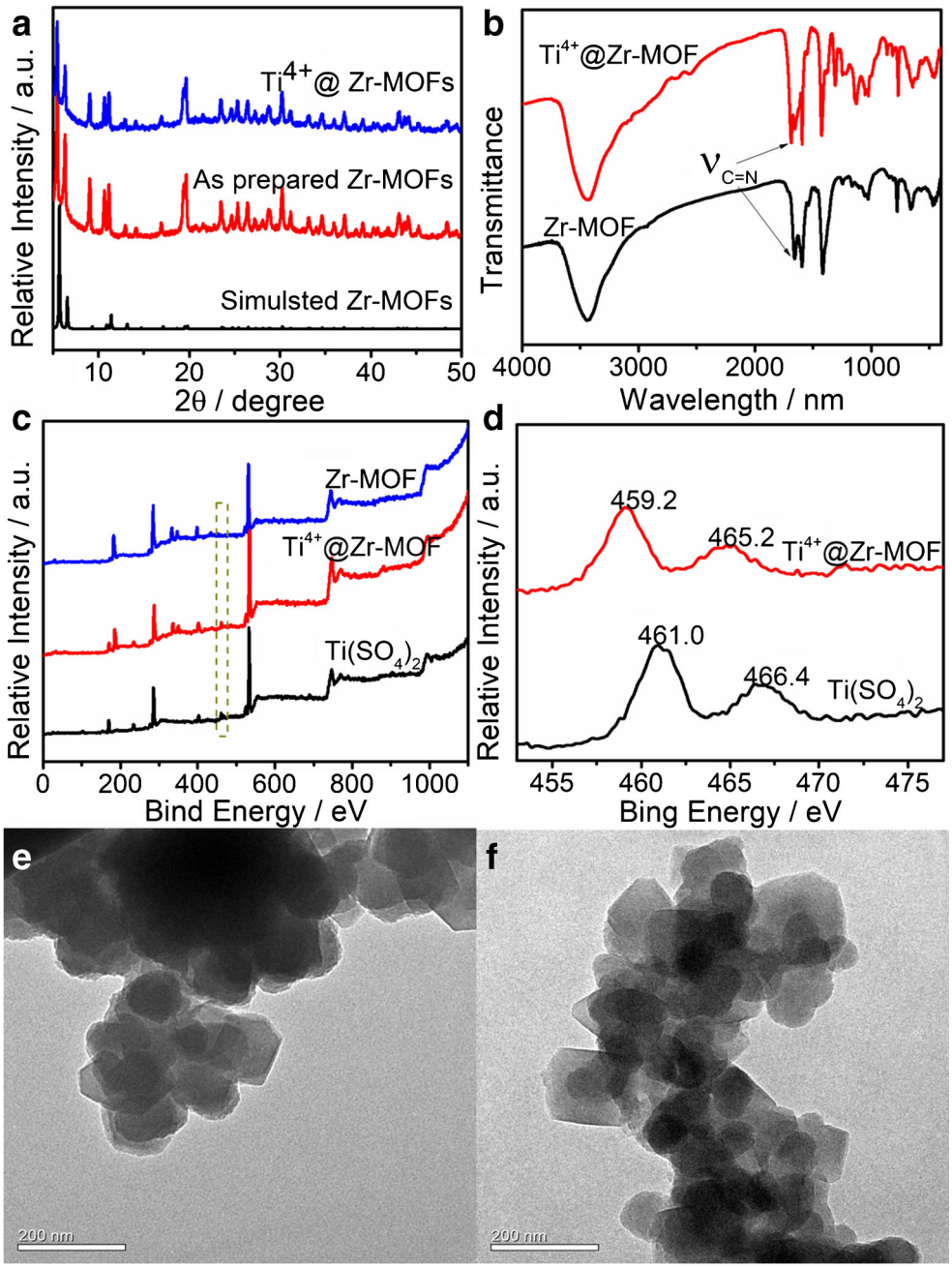

Fig. 1 **a** XRD patterns of Zr-MOF and Ti^{4+}@Zr-MOF; **b** FTIR spectra of Zr-MOF and Ti^{4+}@Zr-MOF; **c** XPS spectra of $Ti(SO_4)_2$, Ti^{4+}@Zr-MOF and Zr-MOF; **d** Ti 2p XPS spectra of $Ti(SO_4)_2$ and Ti^{4+}@Zr-MOF (**e**) TEM images of Zr-MOF; **f** TEM images of Ti^{4+}@Zr-MOF

within Zr-MOF (Fig. 1f). Zeta-potential analysis were also been operated to confirm the introduction of Ti^{4+}. Zeta-potential of Ti^{4+}@Zr-MOF increased from 10.1 mV to 14.0 mV compared to parent Zr-MOF (Fig. S4). Thermogravimetric analysis (TGA) suggests that Ti^{4+}@Zr-MOF still possesses good stability even though Ti^{4+} is introduced into parent Zr-MOF (Fig. S5). For the sake of comparing the capture efficiency of single-metal PPAP with dual-metal PPAP, MIL-125(Ti), MIL-53(Al) and MIL-53(Fe) were also fabricated successfully (Fig. S6 and Fig. S7).

Enrichment of phosphopeptides from standard protein digests

In order to obtain best efficiency, the percentage of TFA (0.5%, 1%, 2%, 4%) within loading buffer and incubation time (10 min, 20 min, 30 min, 40 min) were optimized. As shown in Fig. S8, different percentage of TFA showed different results towards phosphopeptides enrichment. According to the peaks intensities, 2% TFA within loading buffer was selected. With the increment of incubation time before 30 min, the signal intensities are raised significantly (Fig.

S9). Increasing the incubation time from 30 min to 40 min, the peak intensities are increased limitedly. Therefore, 2% TFA within loading buffer and 30 min incubation time were used in subsequent experiment.

To investigate the capture efficiency of Ti^{4+}@Zr-MOF towards phosphorylated peptides through MS analysis, β-Casein digests and α-Casein digests were used as model phosphopeptides. At a concentration of 200 fmol·μL^{-1} β-Casein digests, without enrichment, the signal peaks of low abundance phosphopeptides were severely suppressed (Fig. 2a), and almost no phosphopeptides were detected. After treatment with Ti^{4+}@Zr-MOF, the mass spectra (Fig. 2b) were dominated by phosphorylated fragments with high S/N of 7385 and 12 phosphopeptides were counted. Then, α-Casein digests were also incubated with Ti^{4+}@Zr-MOF. As shown in Fig. S10, a total of 24 phosphopeptides were identified and almost all of the non-phosphopeptides were excluded, which were significantly enhanced compared with the α-Casein digests without enrichment. The above results suggested Ti^{4+}@Zr-MOF possesses high affinity with phosphortlated peptides that is attributed to abundant Ti^{4+} and Zr^{4+} coordination sites. Detailed sequence information of captured phosphopeptides from β-Casein digests and α-Casein digests are shown in Table S2 and Table S3, respectively.

To validate dual-metal centers Ti^{4+}@Zr-MOF has better enrichment performance compared with single-metal MOF, parent Zr-MOF and Ti-based MOF (MIL-125(Ti)), which only contain single metal ions, were also utilized to extract phosphopeptides from β-Casein digests. When treated with

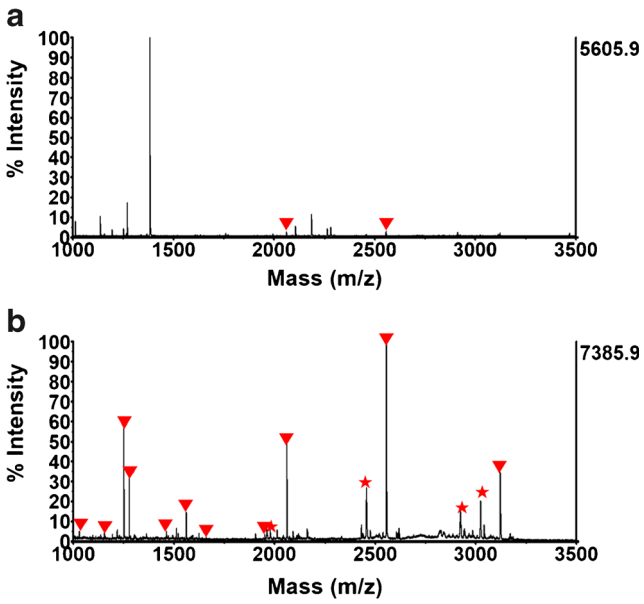

Fig. 2 MALDI-TOF-MS for the phosphopeptides from 200 fmol·μL^{-1} β-Casein digests: **a** before enrichment; **b** after enrichment by Ti^{4+}@Zr-MOF; Phosphopeptides were marked with ▼ and dephosphopeptides were marked with ★

Zr-MOF, although five phosphopeptides were detected (Fig. S11), the peak intensities were low and the spectra had interference of non-phosphopeptides. On the other hand, after treatment with MIL-125(Ti), non-phosphopeptides were observed obviously in the mass spectra (Fig. S12), revealing it had low specificity towards phosphopeptides. The results showed that Ti^{4+}@Zr-MOF was superior to Zr-MOF and MIL-125(Ti) towards phosphopeptides extraction, which is due to the dual-metal synergistic effects within Ti^{4+}@Zr-MOF. Complementary enrichment capability of dual-metal makes Ti^{4+}@Zr-MOF captures more numbers of phosphopeptides.

To further confirm dual-metal synergistic effects play a crucial role in increasing enrichment efficiency of phosphopeptides, Al^{3+}@Zr-MOF and Fe^{3+}@Zr-MOF were fabricated via chelation interaction between bipyridine sites and metal ions. Then they were utilized for assessing the capture efficiency of phosphopeptides from β-Casein digests. Simultaneously, MIL-53(Al) and MIL-53(Fe) that belong to single-metal MOF were also synthesized successfully and used for comparison of enrichment performance with Al^{3+}@Zr-MOF and Fe^{3+}@Zr-MOF correspondingly. Al^{3+}@Zr-MOF and Fe^{3+}@Zr-MOF captured 8 and 9 phosphopeptides with high S/N exceeding 4000 from β-Casein digests, respectively. However, MIL-53(Al) and MIL-53(Fe) only captures 4 and 6 phosphopeptides, respectively (Fig. S13). In comparison with MIL-53(Al) and MIL-53(Fe), more numbers of phosphopeptides captured by Al^{3+}@Zr-MOF and Fe^{3+}@Zr-MOF should also be ascribed to the synergistic effects of the dual metals. Numbers of enriched phosphorylated peptides from standard β-Casein digests by all of the dual-metal MOFs and single-metal MOFs are listed in Table S4. The results clearly present enhanced enrichment efficiency of dual-metal integrated MOF compared with single-metal MOF.

Investigating limitation of detection of phosphopeptides (LOD) is also significant, because phosphorylated peptides are always at low abundance in biosamples. Ti^{4+}@Zr-MOF was incubated with different concentrations of β-Casein digests to test LOD. As depicted in Fig. 3, when the concentration of digests was reduced to 5 fmol·μL^{-1}, 6 phosphopeptide fragments with high signal intensity were determined. Three characteristic peaks of phosphopeptides (m/z = 2061, 2556, 3122) derived from β-Casein can still be observed with an S/N ratio of 25, while the concentration was 1 fmol·μL^{-1}. Even when the concentration was as low as 0.1 fmol·μL^{-1}, phosphorylated fragments (m/z = 2556) were also detected. The ultra-low detection towards phosphopeptides of Ti^{4+}@Zr-MOF is attributed to the abundant metal sites that provide robust interaction with phosphate.

In addition, the interference of other components in biosamples is also one of the main problems for enriching

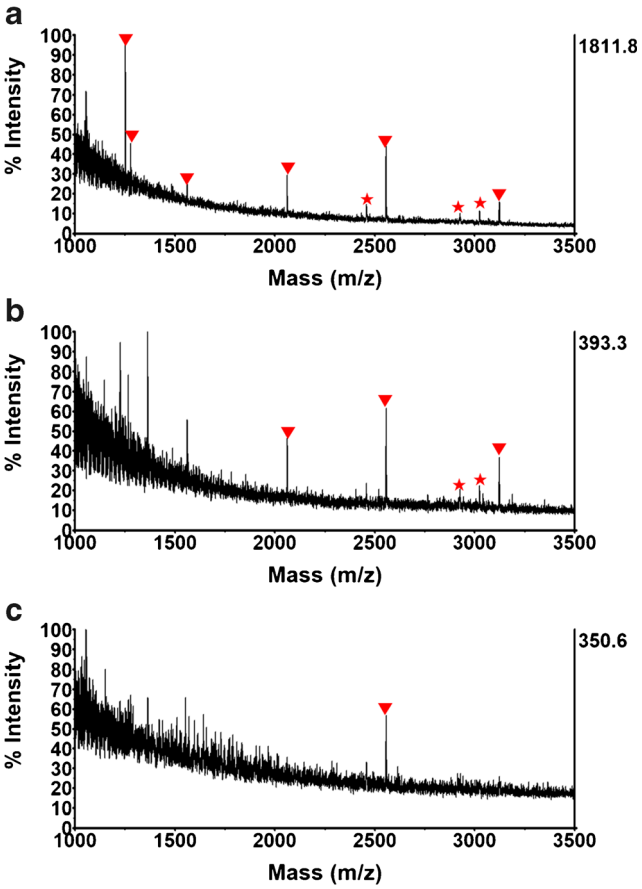

Fig. 3 MALDI-TOF-MS for phosphopeptides enriched by Ti^{4+}@Zr-MOF from β-Casein digests with different concentration: **a** 5 fmol·μL^{-1}; **b** 1 fmol·μL^{-1}; **c** 0.1 fmol·μL^{-1}. Phosphopeptides were marked with ▼ and dephosphopeptides were marked with ★

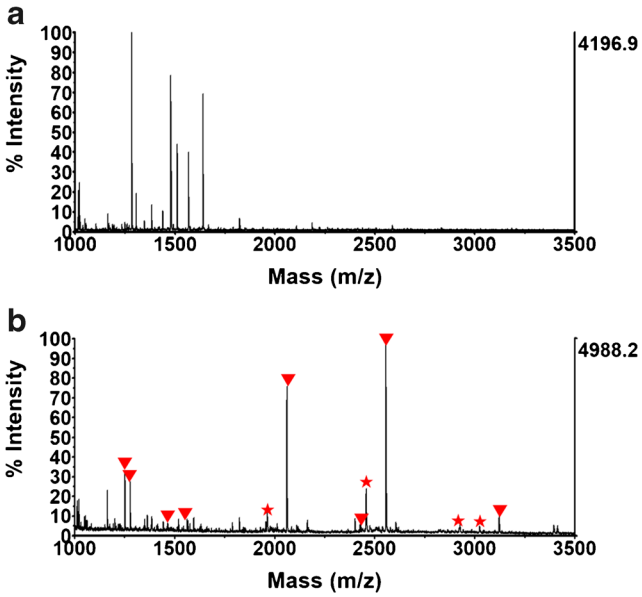

Fig. 4 MALDI-TOF-MS for phosphopeptides from mixture of β-Casein digests and BSA digests at a mass ratio of 1:40: **a** before enrichment; **b** after enrichment by Ti^{4+}@Zr-MOF. Phosphopeptides were marked with ▼ and dephosphopeptides were marked with ★

endogenous phosphopeptides. Although ions, biogenic amines and drugs can be founded in biological organism, they have lower molecular weight compared with peptides. In mass spectra, their signal suppresses phosphopeptide signal insignificantly. In a consequence, non-phosphopeptides having adjacent molecular weight are considered merely. BSA, typical non-phosphorylated protein, was digested and used as the interfering reagents. Phosphopeptides were inhibited completely by the peaks of BSA digests without enrichment (Fig. 4a), when the mass ratio was 40:1 (BSA: β-Casein). After being treated with Ti^{4+}@Zr-MOF, however, the mass spectrum (Fig. 4b) was occupied by phosphopeptides and the peaks of BSA digests were almost vanished. Even when the ratio was increased to 80:1, two phosphorylated fragments were also detected with high intensity (Fig. S14), indicating the high selectivity of Ti^{4+}@Zr-MOF towards phosphopeptides. This is ascribed to strong interaction between metal sites and phosphopeptides and weak affinity with non-phosphopeptides under the optimal buffer condition.

Excluding large molecular proteins and enriching phosphopeptides simultaneously are also crucial, especially for endogenous peptides. Ti^{4+}@Zr-MOF that remains the open 3D frameworks of parent Zr-MOF provides the ability for size-exclusion. Phosphorylated protein (β-Casein, MW = 24,000) and non-phosphorylated protein (BSA, MW = 66,000) were employed as interference proteins to study the size-exclusion effect. As shown in Fig. 5, no phosphopeptides were detected by MALDI-TOF directly, when the mass ratio of β-Casein, β-Casein digests and BSA is 1:800:800. After enrichment, the phosphorylated peptides in the eluent with high intensity appeared in the mass spectra. Notably, the signal of protein was not observed in the eluent (Fig. 5c). In contrast, when the supernatant was analyzed using mass spectrum, the signal of protein was detected successfully. Increasing the ratio of mixture to 1:1000:1000, the mass spectra (Fig. S15) were also occupied by phosphopeptides when the washing buffer was analyzed. These results demonstrate that Ti^{4+}@Zr-MOF with high porosity has the ability of excluding large molecular protein off the composites and enabling the target phosphopeptides to interact with metal sites within the pore.

To evaluate the binding efficiency of the materials, Ti^{4+}@Zr-MOF was utilized for three cycles. As displayed in Fig. S16, the mass spectra were almost identical and have minor loss of phosphopeptides, indicating Ti^{4+}@Zr-MOF has outstanding binding efficiency. To estimate the stability of Ti^{4+}@Zr-MOF, it was utilized for enriching phosphopeptides again after being washed with methanol for several times and exposed to air for one month. As shown in Fig. S17, the mass spectra from β-Casein digests was analogous to that treated with freshly prepared material, confirming

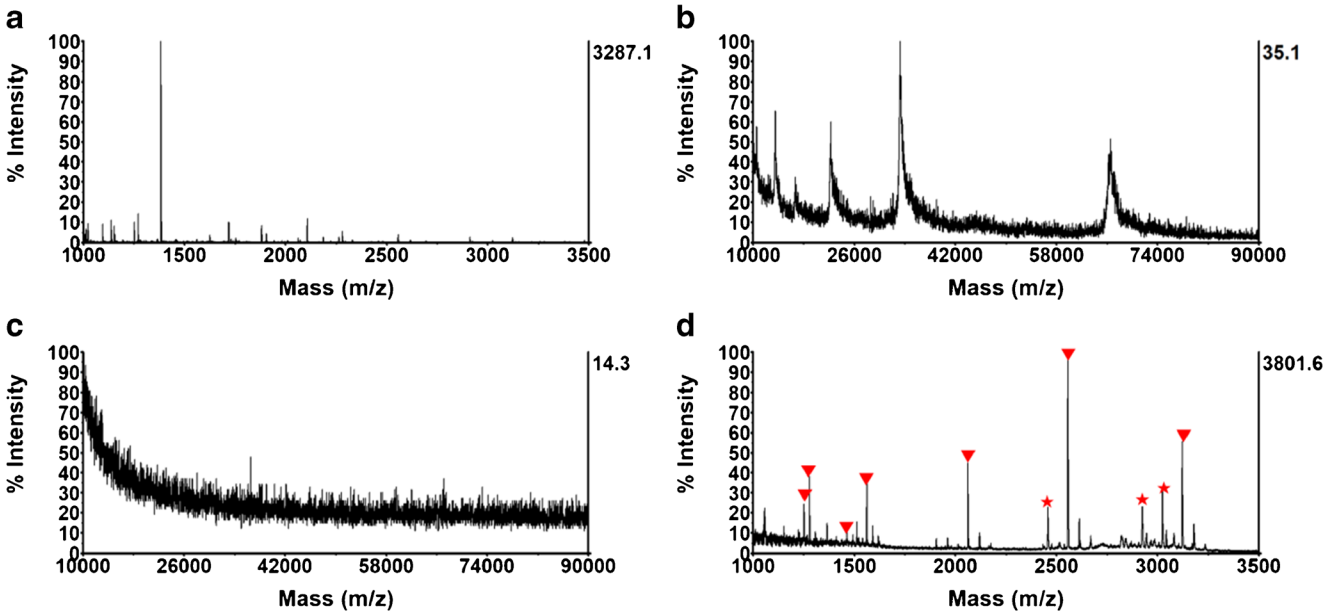

Fig. 5 MALDI-TOF-MS from mixture of intact BSA, intact β-Casein and β-Casein digests at a mass ratio of 1:800:800: **a** without enrichment; **b** supernatant after enrichment by Ti^{4+}@Zr-MOF; **c** and (**d**) elution after enrichment by Ti^{4+}@Zr-MOF. Phosphopeptides were marked with ▼ and dephosphopeptides were marked with ★

the good stability of the material due to robust chelation interaction between bipyridine sites and Ti^{4+}.

Enrichment of phosphopeptides from complex biosamples

Excellent performance of Ti^{4+}@Zr-MOF towards capturing standard phosphopeptides motivates us to utilize the material for enriching endogenous phosphorylated peptides from complex biosamples. Human serum and saliva, both of which belong to clinical specimens and are easy to obtain, were utilized for assessing the enrichment efficiency of Ti^{4+}@Zr-MOF. The eluent were analyzed by MALDI-TOF MS and nano-LC-MS/MS simultaneously. As shown in Fig. S18, for human serum, after treatment with Ti^{4+}@Zr-MOF, four characteristic endogenous phosphopeptides peaks were observed with high intensity when the eluent were analyzed by MALDI-TOF MS. However, the mass spectrum was dominated by non-phosphopeptides before enrichment. The reports of nano-LC-MS/MS also provided the support. Detailed information of captured phosphopeptides from serum is shown in Table S5. The results were identical with the previous work [28].

For human saliva, no phosphorylated peptides were observed without enrichment in the mass spectrum (Fig. 6a). After incubation with Ti^{4+}@Zr-MOF, however, 25 endogenous phosphopeptides were detected by MALDI-TOF MS. MS/MS analysis (Fig. S19) was performed to identify these peaks belongs to phosphopeptides, because mass loss of 98 of the dephosphorylated fragments were observed in the MS/MS spectra in comparison with the corresponding peaks in MS spectra. The reports (Table S6) of nano-LC-MS showed that a total of 105 endogenous phosphopeptides with 55 unique phosphorylated sites were identified directly from human saliva without enzymolysis. The detected phosphopeptides are consisted of 84 mono-phosphopeptides and 21 multi-phosphopeptides.

In order to have an insight into the motif composition of the identified phosphorylated sites from human saliva, we aligned

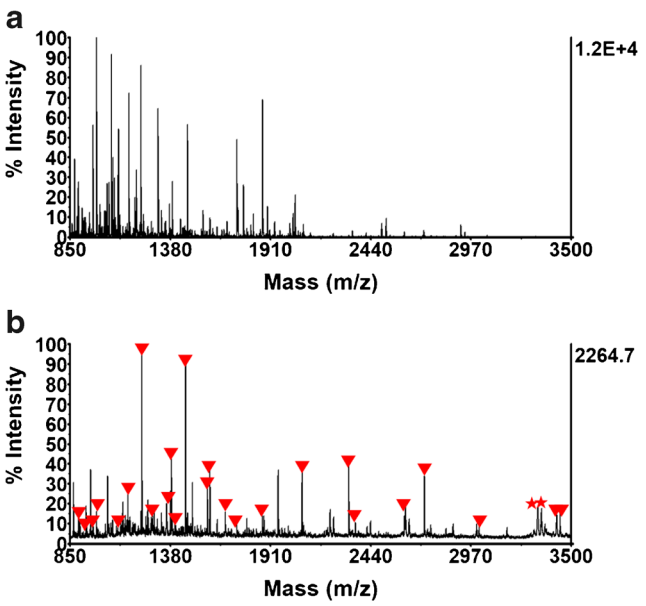

Fig. 6 MALDI-TOF-MS for endogenous phosphopeptides from human saliva without enrichment (**a**) and after enrichment by Ti^{4+}@Zr-MOF (**b**). Phosphopeptides were marked with ▼ and dephosphopeptides were marked with ★

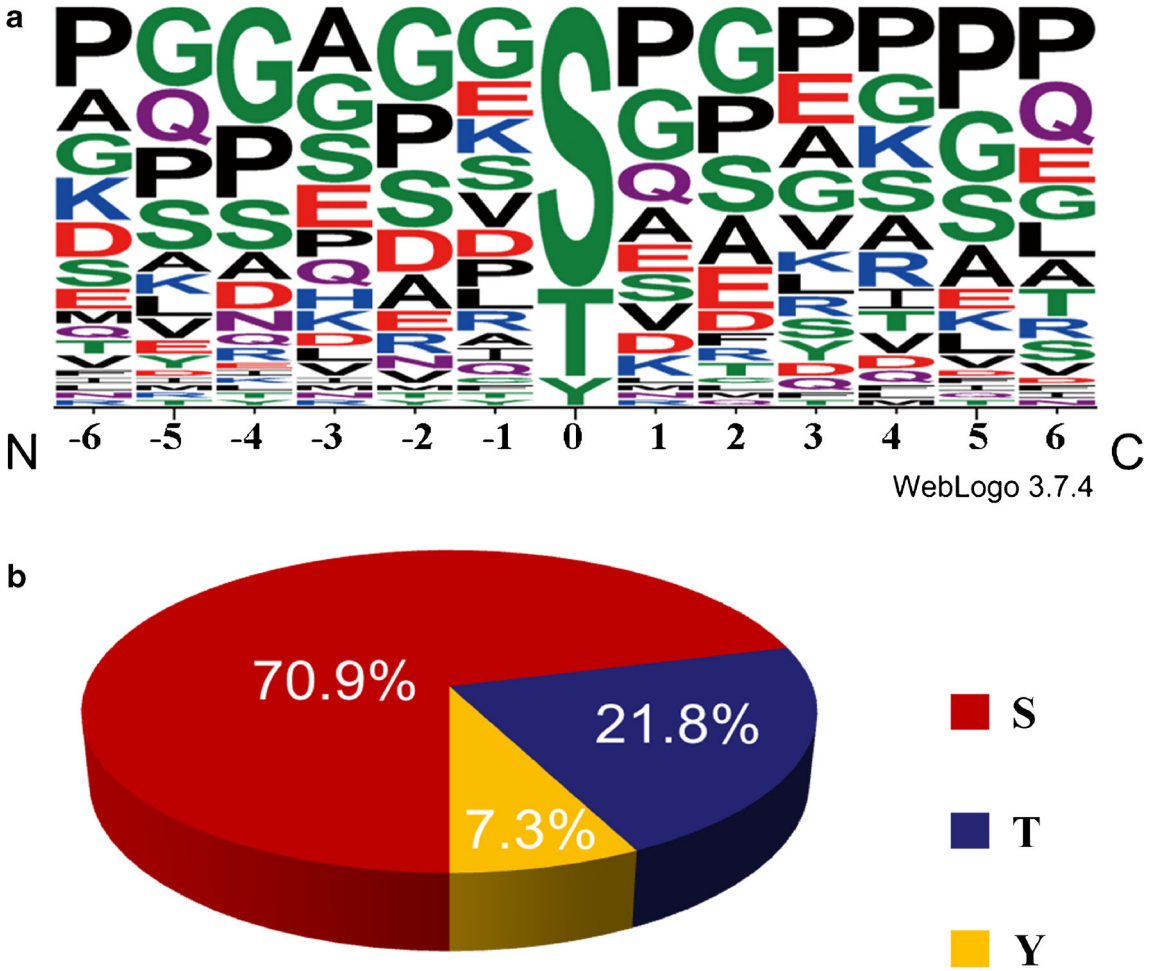

Fig.7 **a** Sequence logo of the motif of the identified phosphorylated sites from human saliva. **b** Distribution of phosphorylated sites in serine, threonine and tyrosine

the amino acid sequence from N-terminal to C-terminal. The conserved sequence patterns were obtained via Weblogo [29]. As shown in Fig. 7, the distributions of identified phosphorylated sites (serine, threonine and tyrosine) were 70.9%, 21.8% and 7.3%, respectively. It was notable that proline appeared frequently on upstream or downstream of phosphorylated sites, which indicates proline-directed motif composition. There also was a high level of glutamic acid that belongs to acidic residue. The above amino acid frequency analysis near the identified phosphorylated sites suggests proline-directed and acidic-directed motif within salivary phosphoproteins that was also reported in previous research [30].

In comparison with other reported materials for phosphopeptides enrichment, results were summarized in

Table 1 The comparison of Ti^{4+}@Zr-MOF with other materials reported previously for extraction of phosphopeptides

Materials	Method	LOD (β-casein)	Specificity (molar ratio of β-casein to BSA)	Size exclusion effect	Practical sample	Numbers of peptides	Ref.
Ti^{4+}@Zr-MOF	IMAC	0.1 fmol	1:80	√	Human saliva	105	This work
T2M	MOAC&IMAC	10 fmol	1:800	×	Human saliva	30	[31]
Ti-PA-MNPs	IMAC	0.8 fmol	1:2000	×	Rat liver lysate	1568	[32]
SiO_2@PDA@Zr-MOF	MOAC	4 fmol	1:1000	√	Human saliva	240	[33]
Fe_3O_4 @mTiO_2-MSA	MOAC	0.05 fmol	1:800	√	Human saliva	307	[34]
Ti^{4+}@PDA@GA	IMAC	–	1:200	×	–	–	[7]
Fe_3O_4@PDA-Ti/Nb	IMAC	2 fmol	1:1000	×	Non-fat milk	19	[15]

Table 1. Ti^{4+}@Zr-MOF has advantages in LOD and size-exclusion effect. Due to the complementary capture capability of Ti^{4+} and Zr^{4+} for phosphopeptides, Ti^{4+}@Zr-MOF performed quite well as sorbents for extracting endogenous phosphopeptides from human saliva. Of course, some challenges remain to be resolved. To detect the lower abundance of phosphorylated peptides, selectivity towards phosphopeptides of the material would be further advanced. In the future work, we will promote the specificity of the method in more complex biosamples.

Conclusion

A dual-metal centered Ti^{4+}@Zr-MOF was fabricated successfully with a novel post-functionalization strategy. The sorbent was applied to capture model phosphopeptides and endogenous phosphopeptides from biological fluids. Ti^{4+}@Zr-MOF exhibits high sensitivity and high selectivity, which is due to the abundant Ti^{4+} and Zr^{4+} coordination sites endowing the sorbent robust interaction with phosphate group of phosphopeptides. The high porosity entrust Ti^{4+}@Zr-MOF with good size-exclusion effect. Remarkably, 4 endogenous phosphorylated peptides and 105 phosphopeptides were extracted from human serum and saliva, respectively. Amino acid frequency analysis near the identified phosphorylated sites from saliva uncovered phosphorylation occurred at proline-directed motifs obviously in salivary proteins. We believe Ti^{4+}@Zr-MOF is promising for large-scale phosphoproteomics and further discovery of disease biomarkers via bioinformatics process.

Acknowledgements This work was supported by the National Key Research and Development Program of China (Project 2016YFA0501401, 2016YFA0501402 and 2017YFA0505003) and the National Natural Science Foundation of China (Project:21974023 and 21475027).

Compliance with ethical standards

Conflict of interest All the experiments in this work were carried out in compliance with the ethical standards, and conducted according to the Declaration of Helsinki and approved by the Ethics Committee of Fudan University.

References

1. Humphrey SJ, Azimifar SB, Mann M (2015) High-throughput phosphoproteomics reveals in vivo insulin signaling dynamics. Nat Biotechnol 33(9):990–995. https://doi.org/10.1038/nbt.3327
2. Liu SQ, Cai X, Wu JX, Cong Q, Chen X, Li T, Du FH, Ren JY, Wu YT, Grishin NV, Chen ZJJ (2015) Phosphorylation of innate immune adaptor proteins MAVS, STING, and TRIF induces IRF3 activation. Science 347(6227):aaa2630. https://doi.org/10.1126/science.aaa2630
3. Olsen JV, Mann M (2013) Status of large-scale analysis of post-translational modifications by mass spectrometry. Mol Cell Proteomics 12(12):3444–3452. https://doi.org/10.1074/mcp.O113.034181
4. Zhou HJ, Ye ML, Dong J, Corradini E, Cristobal A, Heck AJR, Zou HF, Mohammed S (2013) Robust phosphoproteome enrichment using monodisperse microsphere-based immobilized titanium (IV) ion affinity chromatography. Nat Protoc 8(3):461–480. https://doi.org/10.1038/nprot.2013.010
5. Hong YY, Zhan QL, Zheng Y, Pu CL, Zhao HL, Lan MB (2019) Hydrophilic phytic acid-functionalized magnetic dendritic mesoporous silica nanospheres with immobilized Ti^{4+}: a dual-purpose affinity material for highly efficient enrichment of glycopeptides/phosphopeptides. Talanta 197:77–85. https://doi.org/10.1016/j.talanta.2019.01.005
6. Yao YT, Wang Y, Wang SJ, Liu XY, Liu Z, Li YA, Fang Z, Mao JW, Zheng Y, Ye ML (2019) One-step SH_2 superbinder-based approach for sensitive analysis of tyrosine phosphoproteome. J Proteome Res 18(4):1870–1879. https://doi.org/10.1021/acs.jproteome.9b00045
7. Tan SY, Wang JD, Han Q, Liang QL, Ding MY (2018) A porous graphene sorbent coated with titanium(IV)-functionalized polydopamine for selective lab-in-syringe extraction of phosphoproteins and phosphopeptides. Microchim Acta 185(7):316. https://doi.org/10.1007/s00604-018-2846-y
8. Jiang DD, Li XQ, Lv XJ, Jia Q (2018) A magnetic hydrazine-functionalized dendrimer embedded with TiO_2 as a novel affinity probe for the selective enrichment of low-abundance phosphopeptides from biological samples. Talanta 185:461–468. https://doi.org/10.1016/j.talanta.2018.04.006
9. Tseng HC, Ovaa H, Wei NJC, Ploegh H, Tsai LH (2005) Phosphoproteomic analysis with a solid-phase capture-release-tag approach. Chem Biol 12(7):769–777. https://doi.org/10.1016/j.chembiol.2005.05.012
10. Dong MM, Ye ML, Cheng K, Song CX, Pan YB, Wang CL, Bian YY, Zou HF (2012) Depletion of acidic phosphopeptides by SAX to improve the coverage for the detection of basophilic kinase substrates. J Proteome Res 11(9):4673–4681. https://doi.org/10.1021/pr300503z
11. Peng JX, Niu H, Zhang HY, Yao YT, Zhao XY, Zhou XY, Wan LH, Kang XH, Wu RA (2018) Highly specific enrichment of multiphosphopeptides by the diphosphorylated fructose-modified dual-metal-centered zirconium-organic framework. ACS Appl Mater Interfaces 10(38):32613–32621. https://doi.org/10.1021/acsami.8b11138
12. Chen YJ, Xiong ZC, Peng L, Gan YY, Zhao YM, Shen J, Qian JH, Zhang LY, Zhang WB (2015) Facile preparation of core-shell magnetic metal organic framework nanoparticles for the selective capture of phosphopeptides. ACS Appl Mater Interfaces 7(30):16338–16347. https://doi.org/10.1021/acsami.5b03335
13. Gao CH, Bai J, He YT, Zheng Q, Ma WD, Lei ZX, Zhang MY, Wu J, Fu FF, Lin Z (2019) Postsynthetic functionalization of Zr^{4+}-immobilized core-shell structured magnetic covalent organic frameworks for selective enrichment of phosphopeptides. ACS Appl Mater Interfaces 11(14):13735–13741. https://doi.org/10.1021/acsami.9b03330
14. Jayasunder KB, Iliuk AB, Nguyen A, Higgins R, Geahlen RL, Tao WA (2014) Global phosphoproteomics of activated B cells using complementary metal ion functionalized soluble nanopolymers. Anal Chem 86(13):6363–6371. https://doi.org/10.1021/ac500599r
15. Jiang JB, Sun XN, She XJ, Li JJ, Li Y, Deng CH, Duan GL (2018) Magnetic microspheres modified with Ti(IV) and Nb(V) for enrichment of phosphopeptides. Microchim Acta 185(6):309. https://doi.org/10.1007/s00604-018-2837-z
16. Liu QJ, Sun NR, Gao MX, Deng CH (2018) Magnetic binary metal-organic framework as a novel affinity probe for highly selective capture of endogenous phosphopeptides. ACS Sustain Chem

Eng 6(3):4382–4389. https://doi.org/10.1021/acssuschemeng.8b00023
17. Luo B, Yang MG, Jiang PP, Lan F, Wu Y (2018) Multi-affinity sites of magnetic guanidyl-functionalized metal-organic framework nanospheres for efficient enrichment of global phosphopeptides. Nanoscale 10(18):8391–8396. https://doi.org/10.1039/c8nr01914b
18. Peng JX, Zhang HY, Li X, Liu SJ, Zhao XY, Wu J, Kang XH, Qin HQ, Pan ZF, Wu RA (2016) Dual-metal centered zirconium-organic framework: a metal-affinity probe for highly specific interaction with phosphopeptides. ACS Appl Mater Interfaces 8(51):35012–35020. https://doi.org/10.1021/acsami.6b12630
19. Liu GP, Chernikova V, Liu Y, Zhang K, Belmabkhout Y, Shekhah O, Zhang C, Yi SL, Eddaoudi M, Koros WJ (2018) Mixed matrix formulations with MOF molecular sieving for key energy-intensive separations. Nat Mater 17(3):283–289. https://doi.org/10.1038/s41563-017-0013-1
20. Islamoglu T, Ortuno MA, Proussaloglou E, Howarth AJ, Vermeulen NA, Atilgan A, Asiri AM, Cramer CJ, Farha OK (2018) Presence versus proximity: the role of pendant amines in the catalytic hydrolysis of a nerve agent simulant. Angew Chem Int Ed 57(7):1949–1953. https://doi.org/10.1002/anie.201712645
21. Xu XY, Lian X, Hao JN, Zhang C, Yan B (2017) A double-stimuli-responsive fluorescent center for monitoring of food spoilage based on dye covalently modified eumofs: from sensory hydrogels to logic devices. Adv Mater 29(37):1702298. https://doi.org/10.1002/adma.201702298
22. Anik Ü, Timur S, Dursun Z (2019) Metal organic frameworks in electrochemical and optical sensing platforms: a review. Microchim Acta 186(3):196. https://doi.org/10.1007/s00604-019-3321-0
23. Feng L, Yuan S, Zhang LL, Tan K, Li JL, Kirchon A, Liu LM, Zhang P, Han Y, Chabal YJ, Zhou HC (2018) Creating hierarchical pores by controlled linker thermolysis in multivariate metal-organic frameworks. J Am Chem Soc 140(6):2363–2372. https://doi.org/10.1021/jacs.7b12916
24. Yang XQ, Xia Y (2016) Urea-modified metal-organic framework of type MIL-101(Cr) for the preconcentration of phosphorylated peptides. Microchim Acta 183(7):2235–2240. https://doi.org/10.1007/s00604-016-1860-1
25. Li LJ, Tang SF, Wang C, Lv XX, Jiang M, Wu HZ, Zhao XB (2014) High gas storage capacities and stepwise adsorption in a UiO type metal-organic framework incorporating Lewis basic bipyridyl sites. Chem Commun 50(18):2304–2307. https://doi.org/10.1039/c3cc48275h
26. Dan-Hardi M, Serre C, Frot T, Rozes L, Maurin G, Sanchez C, Ferey G (2009) A new photoactive crystalline highly porous titanium(IV) dicarboxylate. J Am Chem Soc 131(31):10857–10859. https://doi.org/10.1021/ja903726m
27. Zhou Y, Yan B (2015) Lanthanides post-functionalized nanocrystalline metal–organic frameworks for tunable white-light emission and orthogonal multi-readout thermometry. Nanoscale 7(9):4063–4069. https://doi.org/10.1039/c4nr06873d
28. Wang JX, Wang YA, Gao MX, Zhang XM, Yang PY (2016) Facile synthesis of hydrophilic polyamidoxime polymers as a novel solid-phase extraction matrix for sequential characterization of glyco- and phosphoproteomes. Anal Chim Acta 907:69–76. https://doi.org/10.1016/j.aca.2015.12.015
29. Crooks GE, Hon G, Chandonia JM, Brenner SE (2004) WebLogo: A sequence logo generator. Genome Res 14(6):1188–1190. https://doi.org/10.1101/gr.849004
30. Stone MD, Chen XB, McGowan T, Bandhakavi S, Cheng B, Rhodus NL, Griffin TJ (2011) Large-scale phosphoproteomics analysis of whole saliva reveals a distinct phosphorylation pattern. J Proteome Res 10(4):1728–1736. https://doi.org/10.1021/pr1010247
31. Wang JW, Wang ZD, Sun NR, Deng CH (2019) Immobilization of titanium dioxide/ions on magnetic microspheres for enhanced recognition and extraction of mono-and multi-phosphopeptides. Microchim Acta 186(4):236–239. https://doi.org/10.1007/s00604-019-3346-4
32. Zhang KN, Hu DH, Deng SM, Han M, Wang XF, Liu HL, Liu Y, Xie MX (2019) Phytic acid functionalized Fe_3O_4 nanoparticles loaded with Ti(IV) ions for phosphopeptide enrichment in mass spectrometric analysis. Microchim Acta 186(2):68–10. https://doi.org/10.1007/s00604-018-3177-8
33. Lin HZ, Chen HM, Shao X, Deng CH (2018) A capillary column packed with azirconium(IV)-basedorganic framework for enrichment of endogenous phosphopeptides. Microchim Acta 185(12):562. https://doi.org/10.1007/s00604-018-3109-7
34. Sun NR, Wang JW, Yao JZ, Chen HM, Deng CH (2019) Magnetite nanoparticles coated with mercaptosuccinic acid-modified mesoporous titania as a hydrophilic sorbent for glycopeptides and phosphopeptides prior to their quantitation by LC-MS/MS. Microchim Acta 186(3):159–158. https://doi.org/10.1007/s00604-019-3274-3